Monthly Notices
of the
ROYAL ASTRONOMICAL SOCIETY

MNRAS **452,** 3273–3280 (2015) doi:10.1093/mnras/stv1420

Observations of PSR J1357−6429 at 2.1 GHz with the Australia Telescope Compact Array

A. Kirichenko,[1,2★] Yu. Shibanov,[1,2★] P. Shternin,[1,2★] S. Johnston,[3] M. A. Voronkov,[3,4,5] A. Danilenko,[1] D. Barsukov,[1,2] D. Lai[6] and D. Zyuzin[1]

[1]*Ioffe Institute, 26 Politekhnicheskaya st., St Petersburg 194021, Russia*
[2]*Peter the Great St Petersburg Polytechnic University, 29 Politekhnicheskaya st., St Petersburg 195251, Russia*
[3]*CSIRO Astronomy, and Space Science, Australia Telescope National Facility, PO Box 76, Epping, NSW 1710, Australia*
[4]*Astro Space Centre, Profsouznaya st. 84/32, 117997 Moscow, Russia*
[5]*School of Mathematics, and Physics, University of Tasmania, GPO Box 252-37, Hobart, Tasmania 7000, Australia*
[6]*Department of Astronomy, Cornell University, Ithaca, NY 14853, USA*

Accepted 2015 June 24. Received 2015 June 22; in original form 2014 August 26

ABSTRACT

PSR J1357−6429 is a young and energetic radio pulsar detected in X-rays and γ-rays. It powers a compact pulsar wind nebula with a jet visible in X-rays and a large-scale plerion detected in X-ray and TeV ranges. Previous multiwavelength studies suggested that the pulsar has a significant proper motion of about 180 mas yr^{-1}, implying an extremely high transverse velocity of about 2000 km s^{-1}. In order to verify this, we performed radio-interferometric observations of PSR J1357−6429 with the Australia Telescope Compact Array (ATCA) in the 2.1-GHz band. We detected the pulsar with a mean flux density of 212 ± 5 μJy and obtained the most accurate pulsar position: RA = $13^{\rm h}57^{\rm m}02\overset{\rm s}{.}525(14)$, Dec. = $-64^\circ29'29\overset{''}{.}89(15)$. Using both new and archival ATCA data, we did not find any proper motion and estimated its 90 per cent upper limit as $\mu < 106$ mas yr^{-1}. The pulsar shows a highly polarized single pulse, as was observed earlier at 1.4 GHz. Spectral analysis revealed a shallow spectral index $\alpha_\nu = 0.5 \pm 0.1$. Based on our new radio position of the pulsar, we discount the claim of an optical counterpart candidate reported previously.

Key words: pulsars: individual: PSR J1357−6429.

1 INTRODUCTION

Born in supernova explosions, neutron stars (NSs) typically obtain velocities orders of magnitude greater than their stellar progenitors. According to statistical analyses (see Hobbs et al. 2005), the mean three-dimensional velocities of NSs, mostly derived from radio data, are about 400 km s^{-1}. The largest firmly established pulsar transverse velocity of 1080 ± 100 km s^{-1}, which has been determined by direct proper motion and parallax measurements with the Very Long Baseline Array (VLBA), belongs to PSR B1508+55 (Chatterjee et al. 2005).

Although an initial kick occurring during supernova explosions is generally accepted as the reason for high velocities, the origin of the kick is currently unclear. Lai, Chernoff & Cordes (2001) discuss several classes of kick mechanisms, but it is not clear whether any of them can explain the fastest moving neutron stars fully (e.g. Chatterjee et al. 2005). Therefore, new detections of high-velocity pulsars are needed to put additional constraints on the models used in the latest supernova explosion simulations (see Wongwathanarat, Janka & Müller 2013). The velocity measurements might also potentially be useful to reveal possible relationships between the velocity and other parameters of NSs (Lai et al. 2001).

PSR J1357−6429 is a young (characteristic age 7.3 kyr) and energetic (spin-down luminosity $\dot{E} = 3.1 \times 10^{36}$ erg s^{-1}) radio pulsar with a period of 166 ms (Camilo et al. 2004). The pulse profile and polarization were studied with the Parkes telescope at 1.4 GHz by Camilo et al. (2004), Johnston & Weisberg (2006), Lemoine-Goumard et al. (2011) and Rookyard, Weltevrede & Johnston (2015). The pulsar field was observed in X-rays, where the pulsar counterpart and a compact tail-like pulsar wind nebula (PWN), implying a noticeable pulsar proper motion, were found (Esposito et al. 2007; Zavlin 2007). Thorough follow-up high-energy studies have revealed X-ray and γ-ray pulsations with the pulsar period (Lemoine-Goumard et al. 2011; Chang et al. 2012). A pulsar plerion extending to a few tens of arcmin was detected in the X-ray and TeV ranges by Abramowski et al. (2011). They also argued that the extended radio emission from the supernova remnant (SNR) candidate G309.8−2.6 (Duncan et al. 1997) is in fact the plerion counterpart.

★ E-mail: aida.astro@mail.ioffe.ru (AK); shib@astro.ioffe.ru (YS); pshternin@gmail.com (PS)

Danilenko et al. (2012) reported the detection of a faint pulsar optical counterpart candidate with the Very Large Telescope (VLT), the position of which was in agreement with the PSR J1357−6429 X-ray position. However, a significant offset (1.54 ± 0.32 arcsec) of the candidate position from the J1357−6429 radio-interferometric coordinates measured 8.7 yr earlier by Camilo et al. (2004) with the Australia Telescope Compact Array (ATCA) raises some doubts about the pulsar nature of the candidate and/or suggests that the pulsar has an extremely high proper motion.

The distance of ∼2.5 kpc to the pulsar was estimated from its dispersion measure $DM = 128.5$ pc cm^{-3} by Camilo et al. (2004). Danilenko et al. (2012) performed an independent distance analysis, comparing the interstellar extinction–distance relation along the pulsar line of sight and the absorbing column density obtained from the X-ray spectral analysis. The resulting distance range of 2.0–2.5 kpc supports the DM distance estimate. The distance range and the candidate offset imply the pulsar transverse velocity to be between 1300 and 2500 km s^{-1}, which is higher than the largest NS velocity measured precisely so far (Chatterjee et al. 2005). A similar velocity range was estimated from comparison of the pulsar X-ray and radio-interferometric positions (Mignani et al. 2011).

Aiming to check whether the pulsar velocity is indeed that high, we performed new radio-interferometric observations with ATCA to obtain a precise pulsar position for another epoch. Another reason for the observations was to extend radio studies of the pulsar itself, which had been investigated only at 1.4 GHz, to a higher frequency range. The details of observations and data reduction are described in Section 2. Our results and reanalysis of the archival data are presented in Section 3 and summarized in Section 4.

2 OBSERVATIONS AND DATA REDUCTION

The observations of the pulsar field were carried out with ATCA on 2013 June 3. The observing session started at 0430 UT and lasted for 9.5 h. The main goal of the observations was to measure the precise position of the source. Therefore, the observations were performed with the 6C array configuration, which has a maximum baseline of nearly 6 km. We used the pulsar binning capability of the Compact Array Broad-band Backend (CABB), which allowed us to perform high time resolution observations (Wilson et al. 2011). The binning mode split the 166-ms pulsar period into 32 independent rotational phase bins. The observations were carried out in the 16-cm band, centred at 2.102 GHz. The total bandwidth of 2.048 GHz was split into 512 spectral channels, providing 4-MHz spectral resolution in the 1.078–3.126 GHz range. PKS B1934−638 was observed at the beginning of the session as a primary standard for the flux density scale and bandpass calibrations. To account for gain and phase instabilities, we observed two nearby secondary calibrators 1329−665 and 1325−55 in a ten-minute loop with the pulsar, where each calibrator was observed for about two minutes. Two calibrators were used to estimate the systematic errors in the position reference frame. Standard data reduction including Radio Frequency Interference (RFI) flagging and calibration was performed with the MIRIAD (**M**ultichannel **I**mage **R**econstruction, **I**mage **A**nalysis and **D**isplay) package (Sault, Teuben & Wright 1995) and KARMA (Gooch 1996) tools were used for data visualization.

The data were split into four 512-MHz sub-bands with central frequencies of 1.334, 1.846, 2.358 and 2.870 GHz. The secondary calibration was then performed separately for each bandwidth partition.

The data were imaged using the MIRIAD *invert* task with the 'robust' parameter set to zero. It provides a trade-off between better signal-to-noise ratio (S/N) and stronger side-lobe suppression in the visibility weighting scheme. The deconvolution process was performed with the *mfclean* routine, which accounts for spectral variations across the bandwidth. For the purposes of absolute astrometry, we used the resulting clean images without further calibration.

Phase self-calibration was performed on the data to improve the image quality. After the first iteration of *mfclean*, model components with flux densities $\gtrsim$1 mJy beam^{-1} were used for the initial multifrequency phase self-calibration, which considerably decreased residual phase errors. Then the weaker sources found on clean images were included in the self-calibration model. As a result, after several clean–self-calibration cycles, the side lobes of field sources became comparable with the thermal noise of ≈50 μJy beam^{-1} for the 1.334-GHz sub-band and ≈25–30 μJy beam^{-1} for the three other sub-bands.

For the lower (1.334-GHz) and higher (2.870-GHz) frequency sub-bands, the synthesized beam sizes were 8.3×5.1 arcsec^2 and 4.5×2.6 arcsec^2, respectively, with position angle $PA \approx -24^\circ$. The ATCA primary beam full width at half-maximum (FWHM) was 42 arcmin for the lowest frequency, decreasing to 15 arcmin for the highest frequency. The selected image size for all sub-bands was $\sim 160 \times 160$ arcmin^2.

To measure the pulsar proper motion confidently, we performed an independent analysis of the available archival ATCA data.[1] The set was obtained on 2000 August 29 in the 6A configuration, with baselines close to those of 6C but in the 1.376- and 2.496-GHz bands, with 128-MHz bandwidths each split into 14 spectral channels (Camilo et al. 2004).[2] The data processing and imaging were similar to those applied to our own set, except that no splitting was performed and the gain calibration was performed with the single observed calibrator 1329−665. The synthesized beam size was 12.7×5.6 arcsec^2 with $PA \approx 48^\circ$ and 7.3×2.2 arcsec^2 with $PA \approx 40^\circ$ for 1.376 and 2.496 GHz, respectively. The imaging procedure for the 1.376-GHz band revealed a point-like source surrounded by concentric side-lobe-like rings that were difficult to clean off. The source is located close to the phase centre and the pulsar and was not identified in the 2013 images. Thorough data inspection showed that it only appears in channels 13 and 14 near the low-frequency side band and thus is likely spurious. Given its proximity to the pulsar, we used only channels 1–12 to eliminate the artefact and its side lobes, which could affect the pulsar position and flux measurements.

3 RESULTS

3.1 The pulsar field

In Fig. 1, we show the self-calibrated image of the pulsar field in the 1.846-GHz sub-band. For comparison, we also present the Molonglo Observatory Synthesis Telescope (MOST) image at 843 MHz with a restoring beam size of ≈104 arcsec (Murphy et al. 2007). Many MOST point-like objects have their firm counterparts in the ATCA image and vice versa. The pulsar is detected with ATCA as a point-like source at 10σ significance in this sub-band and is also visible in the MOST image.

Due to the significantly higher spatial resolution of ATCA, several MOST sources are resolved as groups of separate objects. For instance, a bright extended object near the north edge of the MOST

[1] http://atoa.atnf.csiro.au, project CX001.
[2] The 2.496-GHz data were not reported by Camilo et al. (2004).

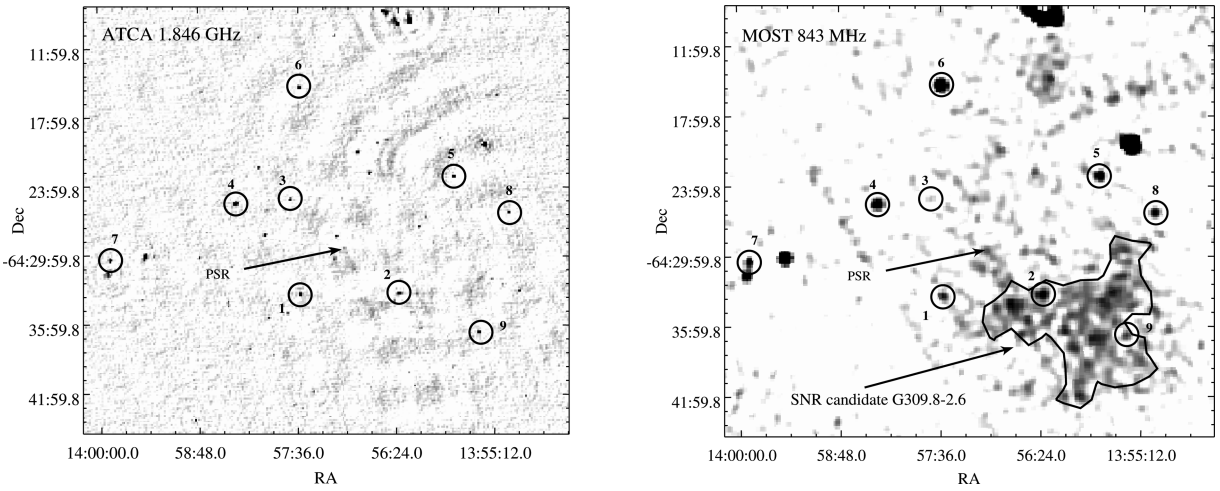

Figure 1. 50 × 50 arcmin^2 field fragment centred on PSR J1357−6429 as visible with the ATCA (left) and MOST (right) at 1.846 GHz and 843 MHz, respectively. The positions of the pulsar and the extended emission from the SNR candidate G309.8−2.6, surrounded by the contour, are indicated by arrows. Numbered circles mark nine bright point-like objects used for relative astrometry of the ATCA images (see text for details).

image is actually a blend of three compact objects. At the same time, insufficient uv-coverage and the long baseline configuration make the interferometer insensitive to large extended structures. That is why the extended emission from the SNR candidate G309.8−2.6 (Duncan et al. 1997) and other extended structures visible in the MOST image cannot be identified in the ATCA image.

The compact north-east–south-west tail-like PWN structure of J1357−6429 visible in X-rays (Chang et al. 2012) is not seen at radio wavelengths.

3.2 The astrometry and pulsar proper motion

To constrain the pulsar proper motion, we used two astrometric methods. The first one, which we refer to hereafter as 'absolute astrometry', allows us to measure source coordinates relative to phase calibrators, the positions of which are known with high accuracy, for instance from very long baseline interferometry (VLBI) measurements. The second approach, which we entitle 'relative astrometry', is based on measurements of the target position shift between observational epochs relative to other sources in the field.

In all cases, to measure the pulsar positions we used on-pulse data obtained from the calibrated visibilities. Using the MIRIAD *psrfix* routine, the pulse-phase bins were phase-adjusted as a function of frequency channel, accounting for the known DM of 128.5 pc cm^{-3} and the pulsar period of 166 ms. After that, a mean off-pulse baseline value was subtracted with the *psrbl* tool. This considerably decreased contamination of the pulsar by the background.

3.2.1 Absolute astrometry

We obtained eight positions of the pulsar in the 2013 images, for each of the four spectral sub-bands in both secondary calibrations. They were determined with the MIRIAD task *imfit* using the object type 'point'. The position uncertainty derived with this task depends slightly on the size of the region around the pulsar where the fit is performed. We used a region of about twice the synthesized beam size in each sub-band. We checked that the resulting positional errors were comparable to the size of the beam divided by twice the S/N. The S/N was ≈11.2, 9.1, 10.8 and 6.4 for 1.334-, 1.846-, 2.358- and 2.780-GHz sub-bands, respectively. To provide better position measurements, the pixel grid on the on-pulse images was adjusted to place the pulsar exactly in the pixel centre. The positions measured in each sub-band were found to be consistent within uncertainties, indicating that no correction for systematic errors between the sub-bands is needed (Deller, Tingay & Brisken 2009).

The mean pulsar positions for 1325−665 and 1329−55 calibrations weighted over the four sub-bands are RA = $13^h57^m02\overset{s}{.}526(15)$, Dec. = $-64°29'29\overset{''}{.}95(15)$ and RA = $13^h57^m02\overset{s}{.}524(14)$, Dec. = $-64°29'29\overset{''}{.}85(12)$, respectively.[3] The best-fitting positions and positional error ellipses are shown in Fig. 2 with crosses and inner thin solid and dashed ellipses for 1325−65 and 1329−55 calibrations, respectively. The positional error ellipse projected on the 1σ coordinate uncertainty represents only a 40 per cent 2D confidence region (e.g. Press et al. 2002). For completeness, we also show 90 per cent confidence ellipses, which are larger in size by a factor ≈2.14. The two measured positions show ≈0.12 arcsec systematic offset in declination. We checked that this is consistent with the shift obtained after cross-calibrating the 1325−665 and 1329−55 standards and measuring their positions. According to Fig. 2, the estimated systematic error along the synthesized beam major principle axis is comparable with the formal statistical 1σ uncertainty. Therefore, the two source positions were weighted by the respective covariance matrices, in order to account for correlations between the errors in RA and Dec., and then combined. The resulting mean position and 40 and 90 per cent uncertainties are shown in Fig. 2 by the bold cross and ellipses. The uncertainties were obtained by adding the estimated systematic covariance matrix to the weighted mean statistical covariance matrix. The final coordinates are RA = $13^h57^m02\overset{s}{.}525(14)$, Dec. = $-64°29'29\overset{''}{.}89(15)$, where the 1$\sigma$ errors correspond to the inner bold ellipse in Fig. 2.

The derived position appears to be different from RA = $13^h57^m02\overset{s}{.}43(2)$, Dec. = $-64°29'30\overset{''}{.}2(1)$ as provided by Camilo et al. (2004) based on the 2000 ATCA 1.376-GHz observations, implying that the pulsar has moved between the 2000 and 2013 epochs.

[3] Herein, the numbers in brackets are 1σ uncertainties referring to the last significant digits quoted; the equinox is J2000.0.

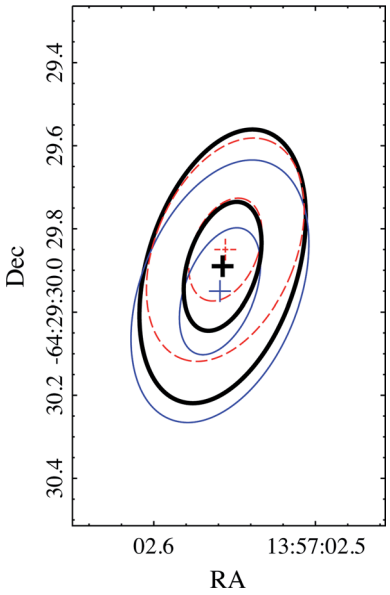

Figure 2. Pulsar position uncertainty ellipses measured at 40 and 90 per cent confidence levels in the 2.1-GHz band. Thin solid and dashed line crosses and ellipses correspond to the calibrations obtained with 1329−665 and 1325−55 standards, respectively. The bold cross and solid bold line ellipses are the derived weighted mean positions.

To check the pulsar shift significance, we remeasured the pulsar position in the 1.376-GHz on-pulse image of the 2000 data, where the pulsar is detected with S/N ≈ 13. At 2.496 GHz, the pulsar is found at a significantly lower S/N, making the position measurements less accurate. The derived 1.376-GHz coordinates are RA = $13^{\rm h}57^{\rm m}02\overset{\rm s}{.}546(76)$, Dec. = $-64^\circ29'29\overset{''}{.}64(55)$.[4] They are consistent with the values stated by Camilo et al. (2004). However, the published position uncertainties appeared to be considerably smaller than the estimate based on the synthesized beam size and pulsar S/N. We thereby conclude that the published pulsar position errors were severely underestimated.

In Fig. 3, we show the pulsar full-band on-pulse images obtained for two epochs using the same calibrator (1329−665). The pulsar positions for the two observational epochs with the respective error ellipses at 40 and 90 per cent confidence levels, which account for the systematics mentioned above, are overlaid on the images. No significant pulsar shift is visible and only an upper limit of ≈1.28 arcsec (90 per cent confidence) can be established. Accounting for that and the time base of 12.76 yr between the two ATCA observations, the 90 per cent upper limit on the pulsar proper motion is $\mu \lesssim 100$ mas yr^{-1}.

3.2.2 *Relative astrometry*

Relative astrometry is generally considered as a more robust tool, which allows us to account for systematic effects that cannot be excluded in advance. For instance, comparing the 2000 and 2013 positions of various sources in the field, we found that they exhibit systematic shifts between the epochs, directed roughly radially from the phase centre and increasing with offset from it. This stretch could result from bandwidth smearing, which was slightly different for pre-CABB and CABB data. There can also be a small rotation

[4] The systematics cannot be accounted for here, since only one secondary calibrator was observed.

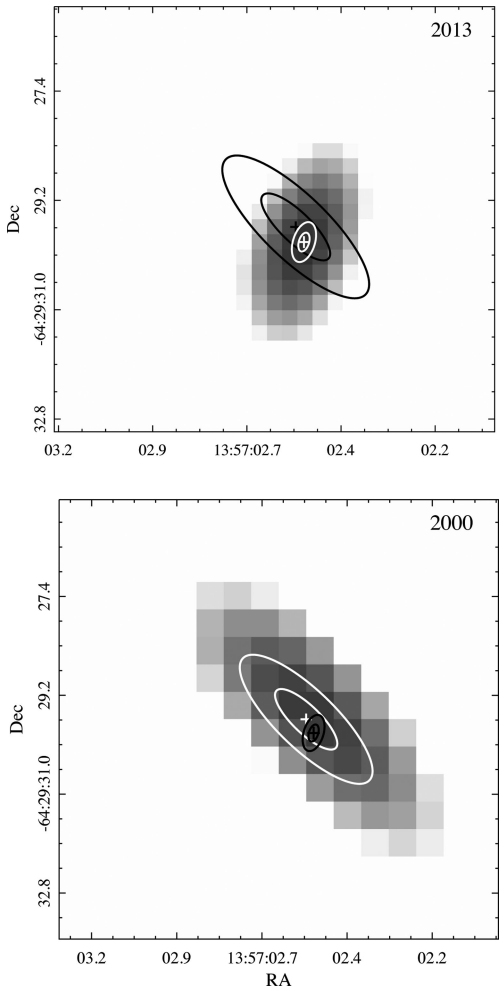

Figure 3. 8 × 8 arcsec^2 ATCA image fragments with PSR J1357−6429 in the centre obtained from non-self-calibrated data at 2.102 GHz in 2013 (*top*) and at 1.376 GHz in 2000 (*bottom*) epochs, using the same calibrator and with pixel scales of 0.25 and 0.5 arcsec, respectively. For a given epoch, the derived pulsar position and the 40 and 90 per cent position uncertainties are shown by the white cross and ellipses, while the black cross and ellipses are related to the other epoch. The images were used for absolute astrometry.

between epochs, caused by the different ephemeris codes used for pre-CABB and CABB correlators.

To increase the image dynamic range and reduce the positional errors, we used the self-calibrated images for each of the 2013 sub-bands, as well as for the 2000 epoch. The pulsar S/N was slightly increased compared with the non-self-calibrated case and was ≈18, 9.9, 11.8 and 8.1 for 1.334-, 1.846-, 2.358- and 2.780-GHz sub-bands, respectively, while in the 2000 image the S/N remained the same. Self-calibration, however, introduced some shift, due to an incomplete sky model. The five images were aligned using a custom-built routine that accounts for shifts, rotations and stretches. For referencing, we used nine relatively bright point-like sources detected in all images with signal-to-noise ratio $\gtrsim$30. They are shown in Fig. 1 and their positions were determined using the *imfit* routine with an accuracy $\lesssim$0.07 arcsec. We found a stretch of a factor of 1.0021(3) and a small rotation of 1.2(6) arcmin for the 2000 image with respect to the 2013 images. Neither significant stretch nor rotation between different sub-bands of the 2013 observations was found. After the transformation, the positions of the reference sources in all images became consistent within the uncertainties.

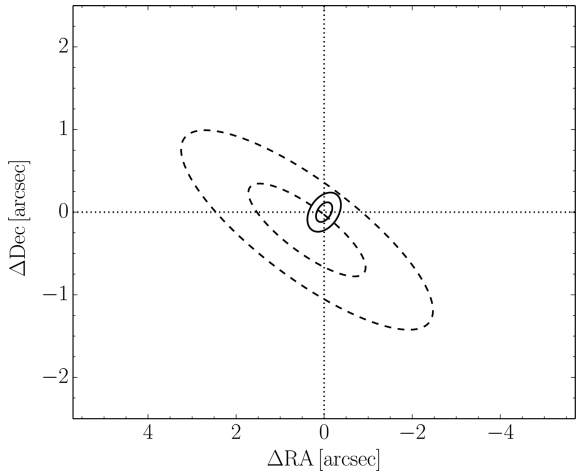

Figure 4. 40 and 90 per cent pulsar position uncertainty ellipses after relative astrometry. The 2013 and 2000 positions are shown by solid and dashed ellipses, respectively. The positions are shown relative to the mean pulsar position at the 2013 epoch. The offsets differ from those presented in Fig. 3 for the absolute astrometry.

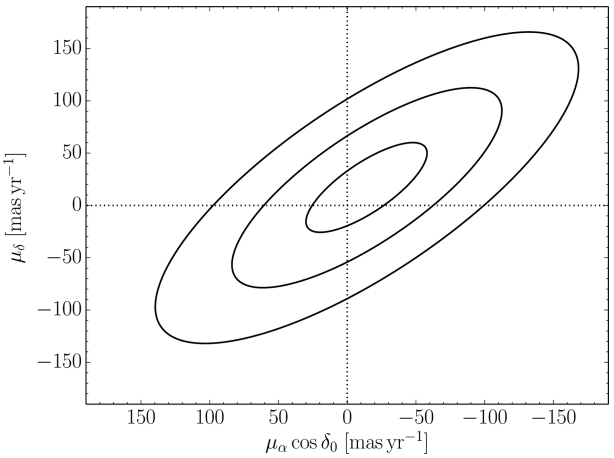

Figure 5. 40, 90 and 99.73 per cent confidence regions of pulsar proper motion based on relative astrometry. $\cos\delta_0 \approx 0.43$, where δ_0 is the declination of the phase centre for the 2013 epoch data.

The pulsar proper motion was included in the routine and was fitted simultaneously with the reference solution.

In Fig. 4, the mean of the pulsar positions in the aligned 2013 sub-bands is compared with the 2000 position. We find that the arrangement of pulsar error ellipses for epochs 2000 and 2013 differs slightly from that provided by the absolute astrometry (cf. Fig. 3), while again no significant shift between the epochs is seen. The 40, 90 and 99.73 per cent confidence regions of the pulsar proper motion $\mu_\alpha \cos\delta_0$ and μ_δ are shown in Fig. 5. The 90 per cent upper limit on the pulsar proper motion, which is the radius of the circular region containing 90 per cent probability, is $\mu < 106$ mas yr^{-1}. This value is compatible with, but slightly higher than, the result obtained from the absolute astrometry. The reason for this is that the positional errors of the 2000 data are in fact underestimated in the absolute astrometry method, since the systematic errors are not accessible. Therefore, we believe that the relative astrometry results are more reliable.

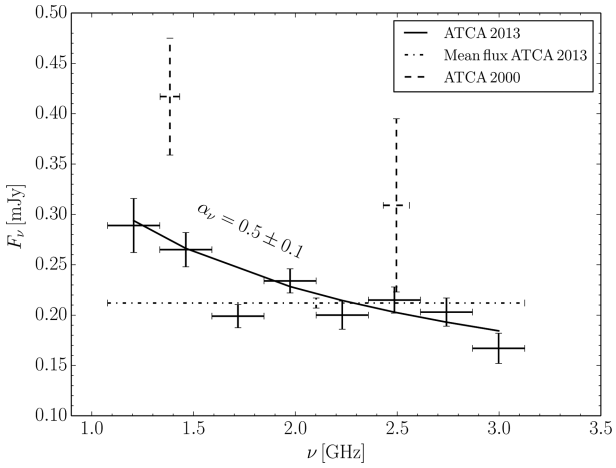

Figure 6. ATCA spectrum of PSR J1357−6429. Solid vertical error bars are the flux densities with 1σ uncertainties in sub-bands shown by horizontal solid bars with 256-MHz widths regularly spaced within the whole 1.1–3.1 GHz band. The line represents the best fit of the measured fluxes by the power law $F_\nu \propto \nu^{-\alpha_\nu}$, with spectral index α_ν shown in the plot. Mean flux densities in the whole 2.102-GHz band measured without division into sub-bands and in 1.376- and 2.496-GHz bands of 2000 are shown by dot–dashed and dashed error bars for comparison. The systematic flux calibration uncertainties of $\lesssim$2 per cent are negligible at this scale.

3.3 The pulsar flux densities and spectrum

To measure the pulsar flux, we used self-calibrated on-pulse visibilities. To study the spectrum in detail, we additionally split each 512-MHz sub-band in half. In order to exclude possible errors introduced by the non-linear cleaning algorithms, we measured the flux directly from the visibility data using the MIRIAD *uvfit* routine. The pulsar position, however, was fixed at the values obtained with *imfit* on the corresponding clean images. The measured fluxes are shown in Fig. 6 by solid error-bar crosses. The mean flux over the full 2013 band is 212 ± 5 μJy. The spectral energy distribution shows a noticeable flux depression at ≈1.7 GHz. The resulting spectrum excluding this point can be fitted by a single power law with a spectral index $\alpha_\nu = 0.5 \pm 0.1$ (reduced $\chi^2 \approx 0.8$). The depression significance in respect of the fit is $\approx 3\sigma$. The inclusion of this point makes the fit unacceptable (reduced $\chi^2 \approx 2.3$). It is hard to explain the depression by any interstellar absorption at the pulsar line of sight, e.g. owing to OH 1.665- and 1.667-GHz lines. There are only three pulsars in which weak OH absorption features with FWHM of 1.5–3 km s^{-1} are observed (e.g. Minter 2005, and references therein). Such features cannot lead to the observed flux depression in our case. In addition, we inspected background objects and found a similar feature at 1.7 GHz in spectra of sources located within ≈2.5 arcmin of the phase centre, while sources located at larger angular distances and the calibrators do not show this feature. Based on this, we suppose that the feature is a systematic artefact and we exclude it from the pulsar spectral fit.[5]

The pulsar fluxes for the 2000 data were measured using the full-band self-calibrated 1.376- and 2.496-GHz visibilities. The respective fluxes of 417 ± 58 μJy and 309 ± 86 μJy are shown in Fig. 6 by dashed error-bar crosses. Given the large uncertainties of the 2000 observations, it is difficult to make any conclusion about the spectral index. However, the 2000 flux values appear to be larger than those of the 2013 data, at least for the lower frequency. The

[5] According to the operation team, the flux depression could be caused by a correlator issue in the pulsar binning mode.

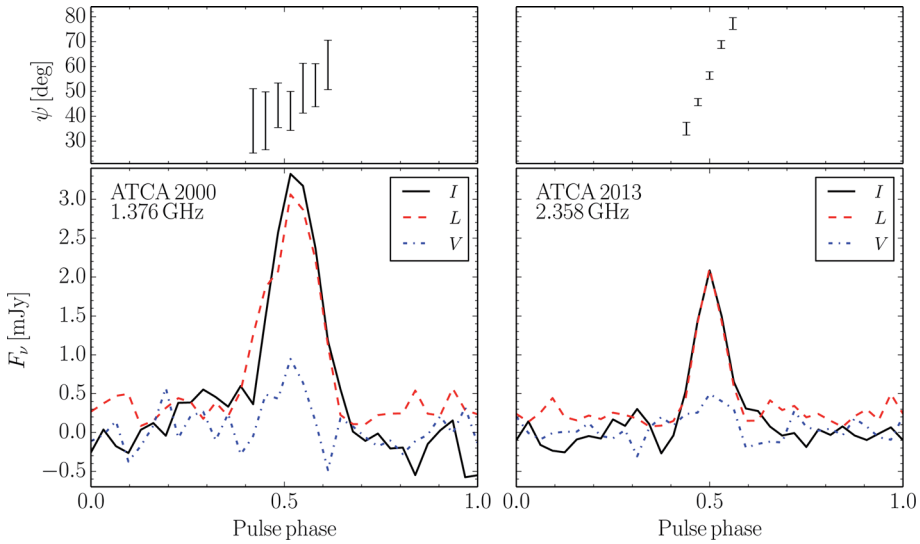

Figure 7. Linear polarization angle ψ (*top*) and pulse and polarization profiles (*bottom*) for PSR J1357−6429 obtained with ATCA at 1.376 GHz (*left*) and 2.358 GHz (*right*). One full period is shown. Solid, dashed and dot–dashed lines show the total intensity I, linearly polarized component $L = (Q^2 + U^2)^{1/2}$ and circular polarization V, respectively. ψ is corrected for RM and shown for on-pulse phases. A phase of 0.5 is placed at the flux density peak.

pulsar flux at 1.376 GHz in the 2000 data differs from that in 2013 by about 2.5σ, including 2 per cent flux calibration uncertainties.[6] The significance of this difference is thus about 99 per cent.

It is possible that the flux variability can be attributed to long-term refractive scintillation (e.g. Lorimer & Kramer 2012). Using the Galactic electron density model NE2001 of Cordes & Lazio (2002), we estimated the field coherence scale $s_0 \approx 4900$ km, the Fresnel scale $l_\mathrm{F} \approx 1.6 \times 10^6$ km and the refractive scale $l_\mathrm{R} = l_\mathrm{F}^2/s_0 \approx 5.2 \times 10^8$ km at 1.376 GHz for the pulsar line of sight. Given that $l_\mathrm{F} \ll l_\mathrm{R}$, the intensity modulation index due to refractive scintillation can be estimated as $m_\mathrm{R} = (s_0/l_\mathrm{R})^{1/6} \approx 0.15$ (Lorimer & Kramer 2012). This value is consistent with the observed 1.376-GHz flux modulation between the two epochs $(F_{2000} - F_{2013})/(F_{2000} + F_{2013}) = 0.16 \pm 0.08$. For the Kolmogorov turbulence spectrum, the modulation index scales with the frequency as $m_R \propto \nu^{0.56}$ and at 2.496 GHz it is larger by a factor of 1.4 than at 1.376 GHz. This is not excluded by the data. The time-scale of the flux variability due to refractive scintillation $\Delta t_\mathrm{R} = l_\mathrm{R}/v_\mathrm{tr}$ is inversely proportional to the pulsar transverse velocity v_tr. Using the derived upper limit on the pulsar proper motion, we estimated the lower limit as $\Delta t_\mathrm{R} \gtrsim 6$ d, which is significantly larger than the duration of our observations.

3.4 The pulse profile and polarization

We studied the pulse and polarization profiles of the 2013 epoch in the same eight 256-MHz sub-bands. The phase-resolved I, Q, U and V Stokes parameters were extracted using the MIRIAD *psrplt* routine. The pulsar emission is observable in five adjacent phase bins. We found no significant profile width and polarization changes across the whole 2.102-GHz band. As an example, the resulting pulse profiles for Stokes I, circular polarization V and linearly polarized component $L = (Q^2 + U^2)^{1/2}$ in the 2.358-GHz sub-band are shown in the lower right panel of Fig. 7. The intensity profile shows a relatively wide single component. The pulse FWHM of $32^\circ \pm 3^\circ$ obtained using a Gaussian profile fit, virtually 100 per cent of the linear polarization and a small amount of circular polarization is fully consistent with the higher time and spectral resolution 1.4-GHz data obtained with the Parkes telescope (Johnston & Weisberg 2006; Rookyard et al. 2015). For completeness, in the lower left panel of Fig. 7 we show the same profiles for the 1.376-GHz band of the 2000 data set. These data demonstrate a somewhat wider intensity profile with FWHM $\approx 43^\circ \pm 4^\circ$. The broader pulse profile observed in the 2000 data can partially result from the DM smearing of $\approx 9^\circ$, due to a spectral resolution twice as low with a channel width of ≈ 9 MHz. The smearing in the 2013 data at the same frequency is less significant, $\approx 4^\circ$, and it does not affect the pulse profiles at higher frequencies. Accounting for the DM smearing and the profile fit uncertainties, the 2000 and 2013 intrinsic pulse widths appear to be consistent.

The large bandwidth of the 2013 data allowed us to infer the rotation measure (RM) along the pulsar line of sight, utilizing the λ^2 dependence of the linear polarization position angle ψ. The latter values and their errors were determined from the Stokes parameters Q and U measured in the five on-pulse phase bins with the *uvfit* routine (as described in Section 3.3) for each of the eight spectral sub-bands. A linear fit to the observed $\psi(\lambda^2)$ dependence was performed in each phase bin, in order to check for possible RM variation with phase (Noutsos et al. 2009). The resulting RM values were found to be consistent within the uncertainties, therefore the global fit for $\psi(\lambda^2)$ dependence was performed with a RM value tied between all five bins. The initial regression was not good, with $\chi^2 = 1.79$ for 34 degrees of freedom, indicating that either position-angle errors were underestimated or a non-trivial spectral behaviour of the position angle exists. Indeed, the data for two lowest frequency bands in our set likely show a shallower swing of ψ than in the other six sub-bands. Since the reason for such behaviour is unclear, we increased the errors of the measured ψ values conservatively to make the χ^2 of the global fit equal to one. The resulting RM of -43 ± 1 rad m^{-2} is smaller, but consistent with -47 ± 2 rad m^{-2} estimated from the Parkes Telescope 1.4-GHz data obtained with a narrow bandwidth (Johnston & Weisberg 2006). We note also that the RM fit for the six upper frequencies is successful without any error renormalization, however this gives a smaller RM of -37 ± 1 rad m^{-2}. Therefore, we cannot exclude

[6] See e.g. http://www.narrabri.atnf.csiro.au/observing/users_guide/html/chunked/ch02s02.html

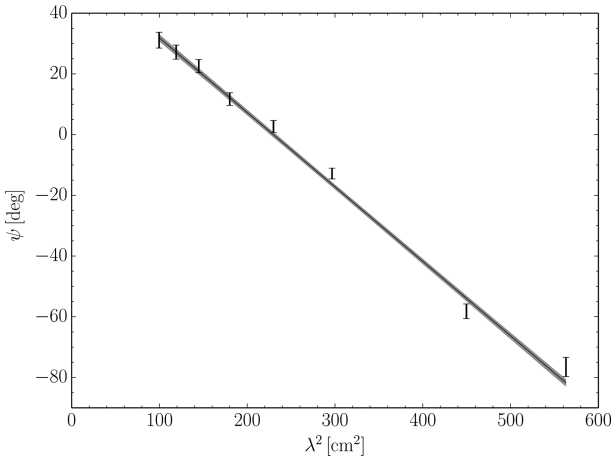

Figure 8. Polarization angle ψ against square of the observing wavelength λ. The grey-hatched region shows 68 per cent linear fit uncertainty.

spectral variations of the RM, as observed for some pulsars (Dai et al. 2015). An illustration of the $\psi(\lambda^2)$ dependence for the central phase bin is shown in Fig. 8. The solid line with grey-hatched region in Fig. 8 shows the best-fitting linear regression with a 68 per cent uncertainty region.

The phase dependence of the position angle in the five on-pulse bins, corrected for the rotation measure, is shown in the top right panel of Fig. 7. This dependence is clearly linear, with slope $C = 0.96 \pm 0.03$. As expected, the results for the 1.376-GHz data of the 2000 observations are consistent with the 2013 measurements (Fig. 7, top left panel). They are also consistent with the higher time resolution data obtained with the Parkes telescope (Rookyard et al. 2015). The ψ-phase dependence demonstrates almost no curvature. Therefore, virtually any pulsar emission geometry can be fitted to the data, according to the classical rotation vector model (RVM: Radhakrishnan & Cooke 1969). Using a more detailed ψ curve, Rookyard et al. (2015) obtained loose constraints on the angle between the magnetic and the rotation axes α. However, the authors favoured the almost-aligned rotator with $\alpha \approx 7^\circ$.

While the RVM does not provide robust constraints on the pulsar emission geometry from our data, it is nevertheless possible to invoke additional arguments based on the observed pulse profile width and statistical data for other pulsars. Gil, Gronkowski & Rudnicki (1984) showed that the half-opening angle of the pulsar beam ρ_q (at a certain relative intensity level q) can be related to the pulse width W_q at the same level via the expression

$$\cos\rho_q = \cos\alpha\cos(\alpha+\beta) + \sin\alpha\sin(\alpha+\beta)\cos(W_q/2), \quad (1)$$

where β is the angle of closest impact of the line of sight to the magnetic axis. In addition, the slope of the positional angle curve at the inflection point is related to the angles α and β via the relation

$$\sin\alpha = C\sin\beta \quad (2)$$

(Komesaroff 1970). Utilizing these equations and the value for the pulse FWHM of $W_{50} = 32^\circ$, we can find the angles α, β and ρ_{50} for any line-of-sight position $\zeta = \alpha + \beta$. The resulting solution varies over a broad range, however the ratio $|\beta|/\rho_{50}$, i.e. the value of the impact parameter in units of the emission cone radius, is tied into the narrow range 0.93–1 for all ζ. Similar solutions with $W_{10} = 70^\circ$ give $|\beta|/\rho_{10} \in (0.77, 1)$. This suggests that the line of sight passes the edge of the beam with rotation of the star. One can try to extract the real value of ρ from statistical data for other pulsars. The diagram of pulse width versus period has a clear low boundary which, in the case of the core component, is thought to represent the value of ρ for orthogonal rotators ($\alpha \approx \pi/2$) with low impact parameters ($\beta \approx 0$) (Rankin 1990; Maciesiak & Gil 2011). In this case, the main source of the difference in the observed width from the minimal value is described by

$$W_{\rm obs} = \frac{W_{\rm min}}{\sin\alpha} \quad (3)$$

(Rankin 1990; Maciesiak & Gil 2011). Using the low boundary from Maciesiak & Gil (2011), we can estimate the inclination angle α to be about 10°, on the basis of W measurements alone. Note that, according to Maciesiak & Gil (2011), this method can overestimate α in close-to-aligned cases (low α). However, it is more likely that the single pulse of PSR J1357−6429 is the cut of the cone component at its side, because of the observed high linear and low circular polarizations (Lyne & Manchester 1988). Maciesiak, Gil & Melikidze (2012) argue that estimate (3) is still applicable for conal profiles, provided impact angle β is small. This is not likely in the case of PSR J1357−6429. Since the relative contributions of profile broadening with α and narrowing with β are not known in advance, we employed the method suggested by Malov & Nikitina (2011). The authors recommend using the mean value of the observed pulse widths W in the sample of pulsars with similar periods as a conservative estimate for twice the value of ρ. The expression (9) from Malov & Nikitina (2011) yields $\rho_{10} \approx 13^\circ$ for the PSR J1357−6429 period. From equations (1) and (2), we again obtained $\alpha \approx 10^\circ$, in accordance with the simple estimate from equation (3) and the favoured solution of Rookyard et al. (2015).

4 SUMMARY

New ATCA observations of PSR J1357−6429 allowed us to detect the pulsar in the 1.1–3.1 GHz band, measure its accurate position, intensity and polarization pulse profiles, derive the RM in a wide frequency range and study the pulsar spectrum. Comparing our results with the archival ATCA 2000 data at 1.376 and 2.496 GHz, we examined the variation of pulsar flux, pulse profile and polarization and constrained the pulsar proper motion.

Based on the ATCA 2013 data, the pulsar has a single pulse component with a constant pulse width of about 32° over the whole 1.078–3.126 GHz frequency range. The radiation has a high, almost 100 per cent, linear polarization, which is typical for young pulsars with $\dot{E} \gtrsim 10^{34}$ erg s^{-1} (Weltevrede & Johnston 2008). We do not detect spectral variation of the linear polarization degree. The pulse profile shape and polarization properties are in agreement with the Parkes telescope 1.4-GHz observations (Camilo et al. 2004; Johnston & Weisberg 2006; Lemoine-Goumard et al. 2011; Rookyard et al. 2015) and ATCA 1.376-GHz observations during 2000. An apparent increase of observed pulse width in the 2000 data set is due mainly to DM smearing caused by the worse spectral resolution. The pulsar spectral energy distribution extracted from the 2013 data demonstrates a shallow spectral index of about 0.5. The ATCA 2000 flux values appear to be larger than those of the 2013 data, at least for the lower frequency. This variability can result from the effects of refractive interstellar scintillation on time-scales significantly larger than the duration of our observations. A detailed monitoring campaign is necessary to check this (e.g. Bhat, Rao & Gupta 1999).

The rotation measure estimate of -43 ± 1 rad m^{-2} is compatible within 2σ with the previous narrow-band measurements, but appears to be more reliable, since it is obtained using a wider frequency range. Based on the derived RM, we estimated the mean

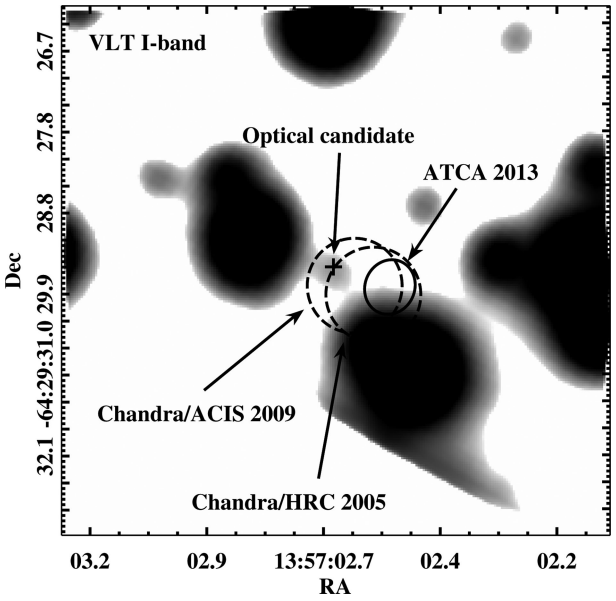

Figure 9. Fragment of the pulsar field imaged with VLT/FORS2 in the *I* band (Danilenko et al. 2012). The pulsar optical counterpart candidate position is shown by the cross. *Chandra* and ATCA pulsar positions are shown by 1σ error ellipses. These ellipses also account for the optical astrometric referencing uncertainty of 0.2 arcsec.

Galactic magnetic field along the pulsar line of sight $\bar{B} = 1.23 \times 10^{-6}$ RM/DM $= -0.41 \pm 0.01$ μG. This is close to the values for most other pulsars from the ATNF catalogue[7] located within a 2° circle around the pulsar position.

On the basis of the absolute and relative astrometry methods, we did not detect proper motion of the pulsar. We estimated a 90 per cent upper limit on it of about 100 mas yr^{-1}, which corresponds to the pulsar transverse velocity $v_{\rm tr} \lesssim 1200$ km s^{-1} if a DM distance of 2.5 kpc is adopted. This does not contradict the value of ~ 650 km s^{-1} suggested by Abramowski et al. (2011) based on the offset of the pulsar from the centre of the extended source HESS J1356−645, possibly associated with the pulsar plerion. The reason why Mignani et al. (2011) and Danilenko et al. (2012) incorrectly suggested the extremely high pulsar transverse velocity was a strong underestimation of the uncertainties in the pulsar radio coordinates derived from ATCA 2000 observations by Camilo et al. (2004). Our analysis shows that further radio observations with at least the same spatial resolution as provided by the ATCA 2013 data will allow us to constrain the pulsar proper motion shift with an accuracy $\lesssim 0.15$ arcsec.

The new ATCA position of the pulsar can be compared with the position of the suggested candidate for the pulsar optical counterpart (Danilenko et al. 2012). The ATCA 68 per cent error ellipse is overlaid on the VLT *I*-band image adapted from Danilenko et al. (2012) and shown in Fig. 9. The pulsar X-ray positions obtained with *Chandra* are also presented. Given the higher accuracy of the ATCA pulsar position compared with the X-ray positions, we conclude that the optical candidate can be discarded as the pulsar counterpart at 99 per cent significance. A relatively bright star is located ∼1 arcsec southwards from the new radio position of the pulsar and further searches for its faint optical counterpart will only be possible with high spatial resolution imaging provided by either the *Hubble Space Telescope* or ground-based optical telescopes with adaptive optics systems.

[7] http://www.atnf.csiro.au/research/pulsar/psrcat/, Manchester et al. (2005)

ACKNOWLEDGEMENTS

We are grateful to the referee Adam Deller for his comments, which prompted us to reconsider certain parts of the manuscript. We thank E. B. Nikitina, I. F. Malov, F. Camilo, Serge Balashev and D. E. Alvarez-Castillo for useful discussions. The work was supported by the Russian Science Foundation, grant 14-12-00316. The Australia Telescope Compact Array is part of the Australia Telescope National Facility, which is funded by the Commonwealth of Australia for operation as a National Facility managed by CSIRO.

REFERENCES

Abramowski A. et al., 2011, A&A, 533, A103
Bhat N. D. R., Rao A. P., Gupta Y., 1999, ApJS, 121, 483
Camilo F. et al., 2004, ApJ, 611, L25
Chang C., Pavlov G. G., Kargaltsev O., Shibanov Y. A., 2012, ApJ, 744, 81
Chatterjee S. et al., 2005, ApJ, 630, L61
Cordes J. M., Lazio T. J. W., 2002, preprint (arXiv:e-prints)
Dai S. et al., 2015, MNRAS, 449, 3223
Danilenko A., Kirichenko A., Mennickent R. E., Pavlov G., Shibanov Y., Zharikov S., Zyuzin D., 2012, A&A, 540, A28
Deller A. T., Tingay S. J., Brisken W., 2009, ApJ, 690, 198
Duncan A. R., Stewart R. T., Haynes R. F., Jones K. L., 1997, MNRAS, 287, 722
Esposito P., Tiengo A., de Luca A., Mattana F., 2007, A&A, 467, L45
Gil J., Gronkowski P., Rudnicki W., 1984, A&A, 132, 312
Gooch R., 1996, in Jacoby G. H., Barnes J., eds, ASP Conf. Ser. Vol. 101, Astronomical Data Analysis Software and Systems V. Astron. Soc. Pac., San Francisco, p. 80
Hobbs G., Lorimer D. R., Lyne A. G., Kramer M., 2005, MNRAS, 360, 974
Johnston S., Weisberg J. M., 2006, MNRAS, 368, 1856
Komesaroff M. M., 1970, Nat, 225, 612
Lai D., Chernoff D. F., Cordes J. M., 2001, ApJ, 549, 1111
Lemoine-Goumard M. et al., 2011, A&A, 533, A102
Lorimer D. R., Kramer M., 2012, Handbook of Pulsar Astronomy. Cambridge Univ. Press, Cambridge
Lyne A. G., Manchester R. N., 1988, MNRAS, 234, 477
Maciesiak K., Gil J., 2011, MNRAS, 417, 1444
Maciesiak K., Gil J., Melikidze G., 2012, MNRAS, 424, 1762
Malov I. F., Nikitina E. B., 2011, Astron. Rep., 55, 878
Manchester R. N., Hobbs G. B., Teoh A., Hobbs M., 2005, AJ, 129, 1993
Mignani R. P., Shearer A., de Luca A., Moran P., Collins S., Marelli M., 2011, A&A, 533, A101
Minter A. H., 2005, BAAS, 37, 1301
Murphy T., Mauch T., Green A., Hunstead R. W., Piestrzynska B., Kels A. P., Sztajer P., 2007, MNRAS, 382, 382
Noutsos A., Karastergiou A., Kramer M., Johnston S., Stappers B. W., 2009, MNRAS, 396, 1559
Press W. H., Teukolsky S. A., Vetterling W. T., Flannery B. P., 2002, Numerical recipes in c++ : the art of scientific computing. Cambridge Univ. Press, Cambridge, NY
Radhakrishnan V., Cooke D. J., 1969, ApJL, 3, 225
Rankin J. M., 1990, ApJ, 352, 247
Rookyard S. C., Weltevrede P., Johnston S., 2015, MNRAS, 446, 3367
Sault R. J., Teuben P. J., Wright M. C. H., 1995, in Shaw R. A., Payne H. E., Hayes J. J. E., eds, ASP Conf. Ser. Vol. 77, Astronomical Data Analysis Software and Systems IV. Astron. Soc. Pac., San Francisco, p. 433
Weltevrede P., Johnston S., 2008, MNRAS, 391, 1210
Wilson W. E. et al., 2011, MNRAS, 416, 832
Wongwathanarat A., Janka H.-T., Müller E., 2013, A&A, 552, A126
Zavlin V. E., 2007, ApJ, 665, L143

This paper has been typeset from a TEX/LATEX file prepared by the author.